Physica Scripta

PAPER

Numerical modeling of the size effect in CdSe/ZnS and InP/ZnS-based Intermediate Band Solar Cells

Asmae El Aouami[1], Kawtar Feddi[2,3], Maykel Courel[4], Francis Dujardin[5], David Laroze[6,*], Laura M Pérez[6], Mimoun Zazoui[7] and El Mustapha Feddi[1,*]

[1] Group of Optoelectronic of Semiconductors and Nanomaterials, ENSAM, Mohammed V University in Rabat, Morocco
[2] REAM Laboratory, UIR, Rabat, Morocco
[3] EIMIS Laboratory, FST, University Abdelmalek Essadi, Tanger, Morocco
[4] Centro Universitario de los Valles (CUValles), Universidad de Guadalajara, Carretera Guadalajara-Ameca Km. 45.5, C.P. 46600 Ameca, Jalisco, Mexico
[5] Université de Lorraine, LCP-A2MC, F-57000, Metz, France
[6] Instituto de Alta Investigación, CEDENNA, Universidad de Tarapacá, Casilla 7 D, Arica, Chile
[7] Laboratory of Condensed Matter and Renewable Energy, Faculty of Sciences and Technology, University of Hassan II Casablanca, Morocco
[*] Authors to whom should be corresponding address.

E-mail: dlarozen@uta.cl **and** e.feddi@um5s.net.ma

Keywords: solar cells, photovoltaic, quantum dots materials, intermediate band, conversion efficiency

RECEIVED
4 October 2020

REVISED
7 December 2020

ACCEPTED FOR PUBLICATION
18 December 2020

PUBLISHED
29 December 2020

Abstract

New generation of solar cells based on the implementation of quantum dots in the intrinsic region has attracted much attention due to the fact to that it takes advantage of photons with energies lower than the band gap for achieving high solar conversion efficiency. However, there is still a need for optimizing many parameters related to the solar cells, such as the size of quantum dots and nature of semiconductor materials. The main objective of this study is to extend the current knowledge of the intermediate band solar cells. In particular, we analyze the effect of dot size on the photonic properties of CdSe/ZnS and InP/ZnS quantum dot solar cells by considering the Schrodinger equation within the effective mass approximation. It is demonstrated that quantum dot size is a critical parameter to be controlled for high efficiency CdSe/ZnS and InP/ZnS quantum dot solar cells. Our results show that open-circuit voltage weakly depends on dot size for both systems while short-circuit current density is increased with dot size increasing. As a result, maximum efficiency values of 31.73% and 32.90% are obtained for CdSe/ZnS and InP/ZnS, respectively under full concentrated light for a dot size of 2.3 nm, thereby demonstrating the potentiality of these proposed heterostructures.

1. Introduction

The conversion efficiency of single junction solar cells is limited to 41% for full concentrated light, and 31% for unconcentrated light [1]. However, and from a thermodynamic viewpoint, the theoretical limit of converted light to electricity is about 93% [2]. Therefore, searching for a new method and architecture to overcome this limit is of enormous interest. One solution to this problem consists of the utilization of multiple semiconductor materials absorbing different regions of the spectral irradiance [3]. This type of device is called multi-junction solar cells. Even if such a design permit higher efficiency, its industrialization is limited due to the complexity and material issues [4]. Another solution consists of adding a band within the band-gap, often known as intermediate band (IB); hence, increasing the number of allowed transitions. This system, called intermediate band solar cells (IBSCs) favors light-to-electricity conversion limit of 63% under ideal conditions [5]. The higher conversion efficiency is a result of the absorption of the extra photons due to valence band (VB)-IB and IB-conduction band (CB) transitions, which enable extra electron-hole pairs to the ones created by direct transitions from the valence band to conduction band [6]. In this sense, the IBSC is able to promote current density of solar cell while keeping the voltage of the device [7]. Quantum dots (QDs) arrayed in superlattice allow the formation of an IB within the

© 2020 IOP Publishing Ltd

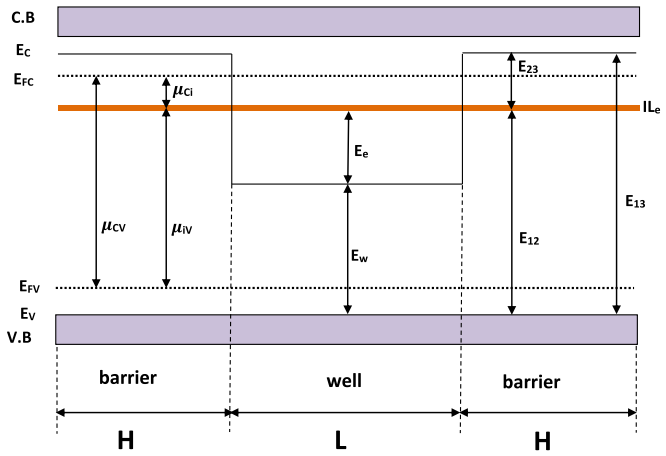


Figure 1. Schematic energy band diagram of the proposed QD-IBSC, where E_e is the ground state electron energy and IL_e is the intermediate level. E_C is the energy of the CB and E_V is the energy of the VB. E_{13} represents its band-gap, while E_W is the band-gap of the quantum dot (CdSe or InP). E_{23} and E_{12} are the energies of top and bottom sub-gaps, respectively. E_{FC} and E_{FV} are the quasi-Fermi levels of CB and VB. Finally, μ_{iV}, μ_{Ci} and μ_{CV} are the chemical potentials between E_{FV} and IL_e, IL_e and E_{FC}, and E_{FV} and E_{FC}, respectively.

valence and conduction bands of the QD material and the band-gap of the matrix material [8, 9]. In ideal cases, the IB is isolated from the bulk material valence and conduction bands, with no participation in the transport of carriers, which results in a negligible impact on quasi-Fermi level position under sunlight. The challenge of the IBSC strategy is to efficiently achieve the demanded energy position of the IB within band-gap of bulk material.

Indeed, since its prediction [5], the IBSC concept has been intensively studied due to the possibility to use photons with energy less than the band gap which make them competitive compared to the classical photodiodes. Thus, they constitute a new field for both experimental and theoretical investigations [10–12]. In theoretical point of view, two simple models are used to describe the intermediate levels. The first one consider that the QDs are sufficiently isolated from each other which leads to discrete energy levels, while the second one suppose that the QDs are quite close and can interact. This model can be described by the Kronig Penney model, which leads to a serie of minibands [13]. the two theoretical approaches demonstrate that the maximum of efficiency can vary from 63.2% by considering one IB to 73% using two IBs. It is worth recalling that the performance of the IBSC is also related to the choice of semiconductor materials. We note that an important number of materials was used in theoretical simulations. Among the most interesting studies, we cite the work developed by Vurgaftman *et al* [14] where the authors have considered direct band gap semiconductors based on $AlAs_xSb_{1-x}$ as a barrier material and InPSb, GaPSb and GaAsSb as QD materials. They have shown that the efficiency reaches 70% by considering two IBs. Jenks [15] have shown that the lattice deformation induced by the mismatch between $Al_yIn_{1-y}As$ QD and $InAs_{1-x}N_x$ barrier material affects considerably the efficiency of the solar cell. A simple overview of the literature show that other QD materials are eventually used, for example $InN/In_xGa_{1-x}N$ [13, 16, 17], $InAs_{0.9}N_{0.1}/GaAs_{0.98}Sb_{0.02}$ [7, 18], $InAs_{1-x}N_x/GaAs_{1-y}Sb_y$ [19], $In_xGa_{1-x}N/GaN$ [20, 21]. Nevertheless, the experimental achievements are still in an embryonic state [12]: some prototypes are already realized using InAs/GaAs-based materials [22–26], GaSb/GaAs [27]. For more details we refer the reader to references [10–12]. Strictly speaking, it is evident that the experimental investigations are still pending with two constraints: performance and cost. In this work, we present an analytical approach for estimating QD-IBSC efficiency, where a selected group of possible materials that will produce IB has been examined. We choose two systems (QD/barrier) CdSe/ZnS and InP/ZnS, because these materials have received an important interest due to their robustness and their large and tunable band gap transitions from UV to IR. It is considering as very important and promising candidate for wide range of optoelectronic devices such as: QLED and photovoltaic devices [28–30]. By precisely controlling the size of the QDs, an optimal current density with high open-circuit voltage (V_{oc}) is obtained, resulting in promoted QD-IBSCs. This work is presented as follows: section 2 covers the electronic and photonic theoretical framework of the QD-IBSC. Results and discussions are presented in section 3, and finally conclusions are introduced in section 4.

2. Theoretical details

2.1. Electronic properties

For calculations, we have considered cubic QDs (wells) forming a lattice embedded into the intrinsic region of a p-i-n junction consisting of ZnS matrix (barrier). This system identified as QD-IBSC is described by two

parameters H and L which indicate the sizes of the barrier ZnS and the QD (CdSe and InP) respectively (see figure 1). The QD energy levels are obtained from the analytical solution of the Schrödinger equation:

$$H\Psi(X,\ Y,\ Z) = E\Psi(X,\ Y,\ Z). \tag{1}$$

Due to the QD shape is cubic, the three-dimensional wave function can be reduced by symmetry consideration and can be written as a function of the three one-dimensional wave functions as follows:

$$\Psi(X,\ Y,\ Z) = \varphi(X) \cdot \varphi(Y) \cdot \varphi(Z). \tag{2}$$

In addition, from the sum of one-dimensional eigenvalues, the total energy E can be obtained:

$$E = E(X) + E(Y) + E(Z). \tag{3}$$

Under the effective mass approach, the Hamiltonian of an electron in QDs is given in one direction as follows:

$$H(X) = -\frac{\hbar}{2m^*}\nabla_X^2 + V_w, \tag{4}$$

where one-directional confinement potential can be written as [31]:

$$V_w = \begin{cases} 0, & \text{if } |X| < L/2 \\ V_0, & \text{if } |X| \geqslant L/2 \end{cases}. \tag{5}$$

Since all three axes (X, Y, and Z) are equivalent, we can limit our calculations of E to the case of one direction, and it can be found after considering boundary conditions given by the Ben-Daniel-Duke equations [32]:

$$[\varphi_{well}(X)]_{X=\pm L/2} = [\varphi_{barrier}(X)]_{X=\pm L/2}, \tag{6}$$

$$\left[\frac{1}{m^*_{well}} \cdot \frac{d\varphi_{well}(X)}{dX}\right]_{X=\pm L/2} = \left[\frac{1}{m^*_{barrier}} \cdot \frac{d\varphi_{barrier}(X)}{dX}\right]_{X=\pm L/2}. \tag{7}$$

The mixture of equations (6) and (7) yields to the following expression [33]:

$$\tan\sqrt{\frac{m^*_{well}E(X)L^2}{2\hbar^2}} = \sqrt{\frac{m^*_{well}}{m^*_{barrier}}\left(\frac{V_0 - E(X)}{E(X)}\right)}. \tag{8}$$

The solution of equation (8) enables defining the state energy $E(X)$ of the particle.

2.2. Photonic properties

In QD-IBSC, the net photogenerated current density is given by:

$$\begin{aligned} J = q[&F_s n_s N(E_{13},\ \infty,\ T_s,\ 0) + (1 - F_s n_s)N(E_{13},\ \infty,\ T_a,\ 0) \\ &- N(E_{13},\ \infty,\ T_a,\ qV) + F_s n_s N(E_{23},\ E_{12},\ T_s,\ 0) \\ &+ (1 - F_s n_s)N(E_{23},\ E_{12},\ T_a,\ 0) - N(E_{23},\ E_{12},\ T_a,\ \mu_{Ci})], \end{aligned} \tag{9}$$

where F_s is the concentration factor, q is the electric charge of electron, n_s is a geometric factor, T_s is the Sun temperature (6000K), T_a is the room temperature (300K), the quasi-Fermi energies separation is qV, μ_{Ci} is the chemical potential between CB and IL_e, and N is the photon flux density, given by [34]:

$$N(E_l,\ E_u,\ T,\ \mu) = \frac{2\pi n_s}{h^3c^2}\int_{E_l}^{E_u}\frac{E^2}{e^{\frac{E-\mu}{k_BT}} - 1}dE, \tag{10}$$

where E_u is the upper energy limit and E_l is the lower energy limit, T the temperature and μ the chemical potential, while k_B, h, and c are fundamental constants.

Photons with energy $E_{23} < h\nu < E_{12}$ are absorbed, permitting the excitation of electrons from the VB to the CB. In particular, photogenerated carriers with energy higher than E_{23} and lower than E_{12} will thermalize to the band edges. This thermalization value is minimal compared to bulk solar cells, implying that the absorption of photons with energy $E_{23} < h\nu < E_{12}$ is equivalent to the absorption of photon with energy E_{23}. With the absorption of photons with energy $E_{12} < h\nu < E_{13}$, electron transitions from the IL_e to the CB occur. In this case, photogenerated carriers with excess energy thermalize to the band edges as well. On the other hand, the absorption process also takes place for photons with energy $h\nu > E_{13}$. However, the absorption of photons with energy $h\nu > E_{13}$ is equivalent to the absorption of photons with energy E_{13} due to the thermalization of hot carriers.

Considering that the current entering the IL_e should be equal to the one leaving the IL_e, the QD-IBSC current density is expressed as follows:

Table 1. Material parameters of InP, CdSe and ZnS: effective masses for electron m_e^*, band-gap energy E_g [36].

	m_e^*/m_0	E_g (eV)
InP	0.08	1.35
CdSe	0.13	1.675
ZnS	0.2	3.726

$$q[F_s n_s N(E_{23}, E_{12}, T_s, 0) + (1 - F_s n_s) N(E_{23}, E_{12}, T_a, 0) - N(E_{23}, E_{12}, T_a, \mu_{Ci})] = q[F_s n_s N(E_{12}, E_{13}, T_s, 0) + (1 - F_s n_s) N(E_{12}, E_{13}, T_a, 0) - N(E_{12}, E_{13}, T_a, \mu_{iV})]. \quad (11)$$

The solar cell voltage can be calculated from the chemical potentials as follows [35]:

$$qV = \mu_{CV} = \mu_{Ci} + \mu_{iV}. \quad (12)$$

The intensity of light on the QD-IBSC is determined by the number of suns, being 1 sun (F_s=1) the standard intensity at the Earth's atmosphere surface. In this sense, the incident power on QD-IBSC is calculated by:

$$P_{in} = n_s \sigma_s T_s^4 = 1587.2\ W/m^2. \quad (13)$$

where σ_s is the Stefan-Boltzmann constant. Ideally, the maximal concentration case can be obtained for $F_s = \frac{1}{n_s} = 46296$. The QD-IBSC efficiency depends on P_{in} and consequently on the concentration level F_s. In this work, the concentrated light condition of $F_s n_s = 1$ is assumed. The QD-IBSC efficiency can be written as [16]:

$$\eta = \frac{V_{oc} \times J_{sc} \times FF}{P_{in}} = \frac{J_{\max} \times V_{\max}}{F_s \times 1587.2}, \quad (14)$$

where V_{oc} is the open circuit voltage, J_{sc} is the short circuit current density, FF is the fill factor, defined as $FF = \frac{J_{\max} \times V_{\max}}{J_{sc} \times V_{oc}}$, $V_{\max}$ and $J_{\max}$ are the voltage and current density, respectively, corresponding to the maximum power point of the QD-IBSC. After mathematical theories and hypotheses presented in previous sections for the detailed analysis of the material, section 3 states some characteristics of the QD-IBSC performance for one IL case.

3. Results and discussions

In this section, the different energy transitions E_{12}, E_{23} and E_{13}, short circuit photo-generated current density (J_{sc}), open-circuit voltage (V_{oc}), generated current density at the maximum power point ($J_{\max}$), the voltage at the maximum power point ($V_{\max}$), output power (P_{out}), and conversion efficiency (η) of CdSe/ZnS and InP/ZnS QD-IBSCs are discussed. All physical parameters of material systems using in our calculations are presented in table 1. In all calculations $H = 5$ nm.

We start our study by examining the impact of QD-size on the ground state energy of electron (E_e), as can be seen in figure 2. It can be remarked that the first state of electron reduces with the QD-size increasing, as a result of the quantum confinement effect, as electrons are more confined in small QD sizes and tends to the bottom of the potential well as the sizes increase. We can remark also that E_e is more confined in the case of InP/ZnS than the case of CdSe/ZnS, and this can be explained by the difference in V_0 values, which has a direct relation with the band-gaps of the well materials (E_g(InP) = 1.35 eV and E_g(CdSe) = 1.675 eV). For a fixed host material, the more band-gap value of the well material is large, the less potential well is deeper.

Figure 3 shows the optical transition E_{12}, which occurs between the valence band and the ground state energy of the electron. The curves confirm that the inter band transition energy E_{12} decrease while L increases, which can be explained by the effect of low quantum confinement in wider QDs. In fact, as L increases, the fundamental state of the electron becomes closer to the bottom of the potential well, and thus, it influences the value E_{12}.

The opposite behavior is appearing for E_{23}. As shown in figure 4, the optical transition E_{23}, which occurs between he IL_e and the CB, increases as increasing the QD-size. This transition is of enormous importance for the device's efficiency, as it allows us to absorb low energy photons, which has not been possible in conventional solar cells. The difference in curves tendency between CdSe/ZnS and InP/ZnS is due to the diversity in band-gap values. In addition to these transitions, there is the conventional transition E_{13}, which occurs between the CB and the VB, and it is not affected by the size of the QD, as it depends only on the chosen host material.

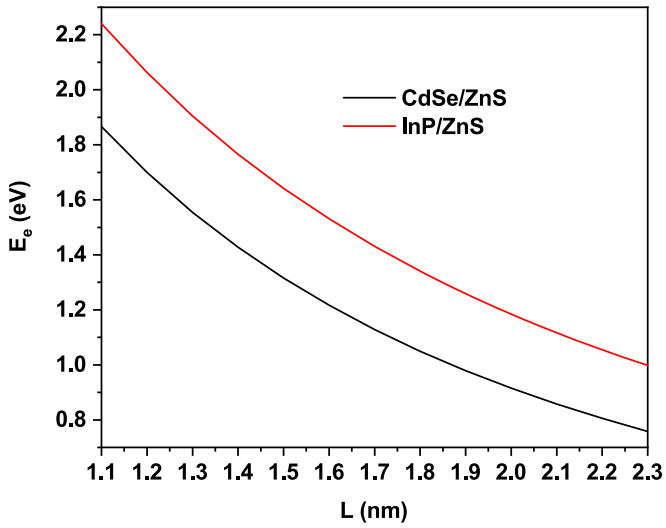


Figure 2. Electron ground state energy as function of *L*.

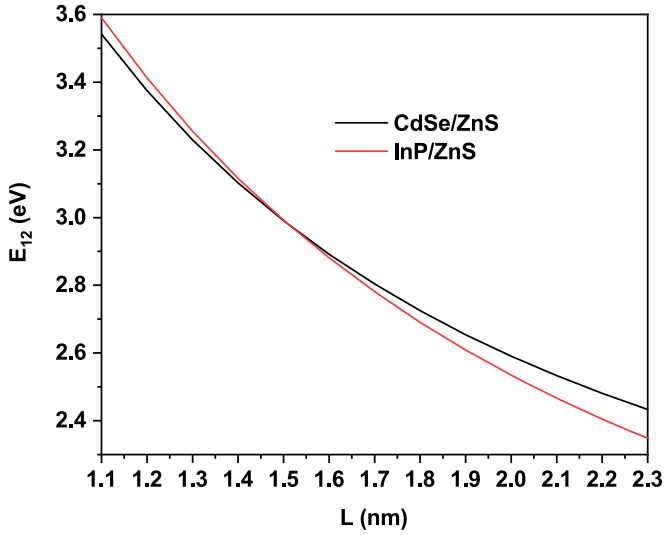


Figure 3. Variations of the sub-gap E_{12} versus QD size *L*.

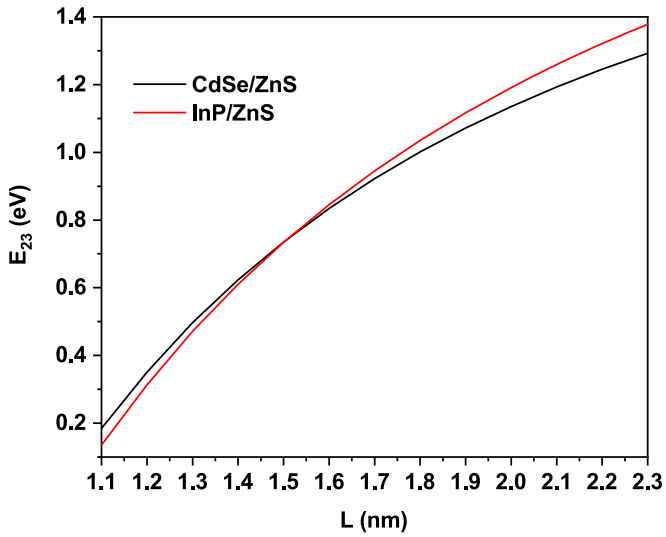


Figure 4. Variations of the sub-gap E_{23} versus dot size *L*.

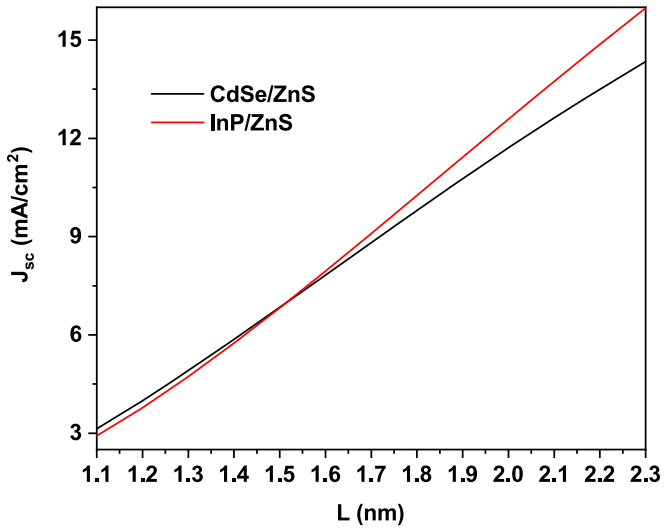


Figure 5. Current density versus QD size *L*.

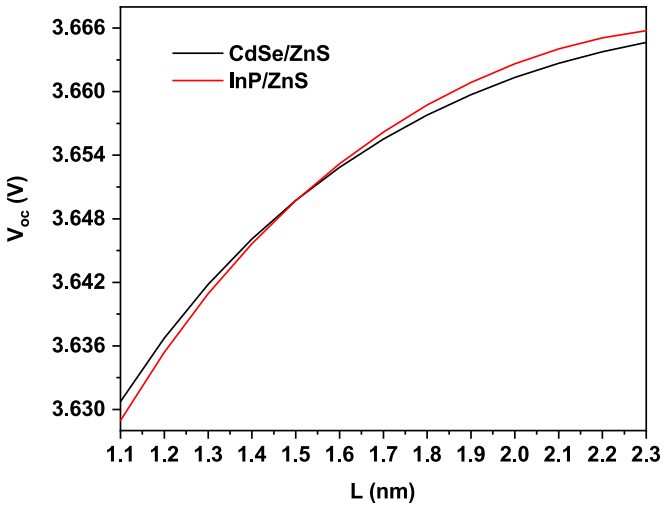


Figure 6. Open-circuit voltage variation versus the dot size *L*

The variation of J_{sc} as a function of the dot size L is presented in figure 5. It is pointed out that for a given H, J_{sc} increases while increasing the dot size L for the both configurations, This behavior can be explained by the fact that the IL_e position is affected by increasing the dot size L, thus the sub-band gaps E_{12} and E_{23} are influenced as depicted in figures 3 and 4. More photons are absorbed while increasing L, Consequently, the photo-generated current density J_{sc} increases. As shown in figure 6, for the both systems, the open circuit voltage V_{oc} weakly depends on L at fixed H, because the variation of L does not affect the transition E_{13}, but the quasi-Fermi levels of CB and VB are slightly affected by varying the dot size L.

Now for the critical parameter of the QD-IBSC, which is the photovoltaic conversion efficiency (η), is depicted in figure 7 as a function of different QD-sizes. We can observe that the conversion efficiency increases as a function of L. One important remark is that in the current study, we have considered only the impact of one IL_e, and we have limited our calculations to the case where no second IL_e is observed. The increased efficiency is due to the added transitions (E_{23} and E_{12}) alongside conventional transition E_{13}. As the QD-size increases, more photons are absorbed, thus, increasing the photo-generated current density. The same curves tendency is observed for both CdSe/ZnS and InP/ZnS materials. The only difference is in the value of the maximum efficiency, which is $\eta = 31.73\%$ for CdSe/ZnS and $\eta = 32.90\%$ for InP/ZnS under full concentrated light. The maximum efficiency is achieved for $L = 2.3$ nm. The attained efficiencies are still far from the maximum

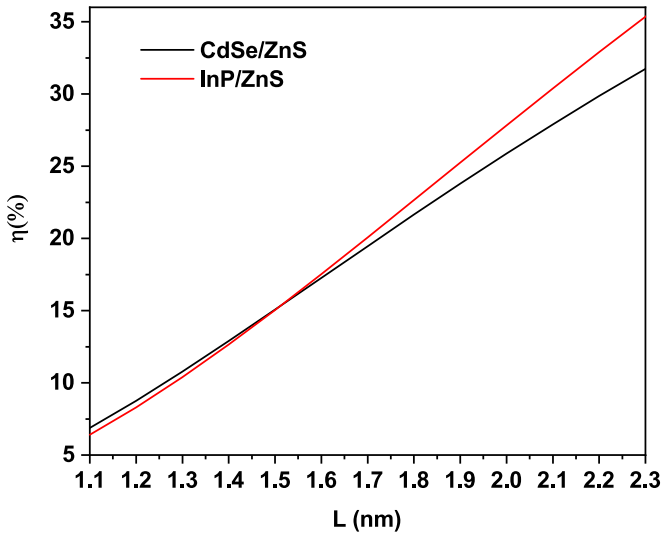


Figure 7. Photovoltaic conversion efficiency dependance on QD size L.

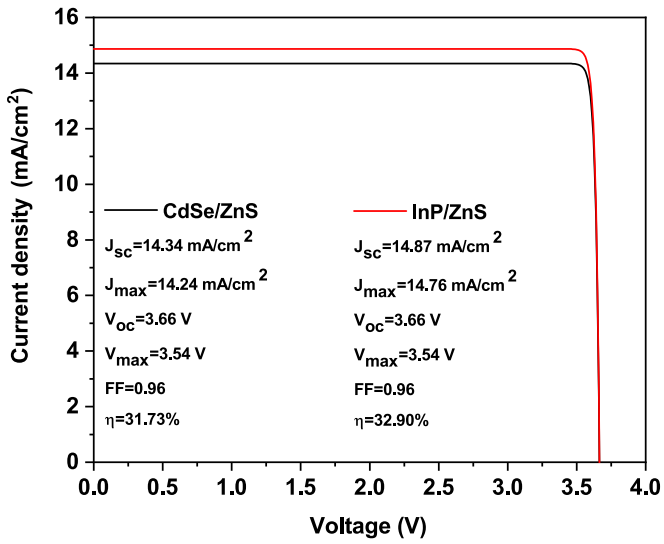


Figure 8. Current density versus voltage for $L = 2.3$ nm.

efficiency of QD-IBSC, and this is because the chosen materials combinations are not optimum. As is was recommended by Levy *et al* [37], an efficiency of more than 60% can be achieved if:

1. The host material band-gap is in the range of 1.43 eV $< E_g <$ 2.65 eV.
2. The valence band offset is negligible.
3. The conduction band offset must be higher than $0.48E_g - 0.22$.
4. The lattice mismatch between well and barrier materials is more than 1%.

In figure 8, the current-voltage characteristics of the QD-IBSCs are presented. The primary parameters that define the device properties are depicted. It can be observed that the generated current density for the case of InP/ZnS is more than the one of CdSe/ZnS. Such a difference is due to the diversity in the values of optical transitions E_{12}, E_{23}, and E_{13}. For the output power, as shown in figure 9, it increases with respect to the voltage, until reaching a maximum and then rapidly decreases. The maximum power point is the one that delivers the maximum efficiency of the device. The same behavior is observed for both considered materials. The only difference in the maximum efficiency due to the different generated current density is observed.

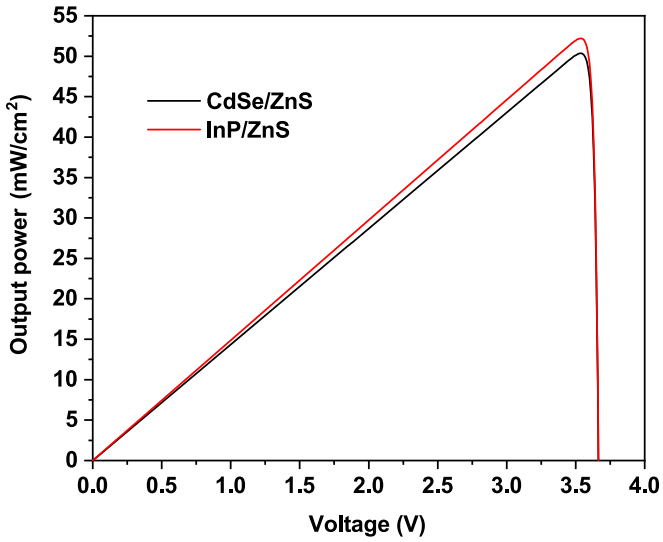


Figure 9. Output power versus voltage for $L = 2.3$ nm.

4. Conclusion

In this paper, the potentiality of introducing CdSe/ZnS and InP/ZnS quantum dots into solar cells was theoretically analyzed. The behavior of InP/ZnS and CdSe/ZnS multiple QD-IBSCs was examined by employing an analytically method, under the approximation of the effective mass. Particularly, the quantum dot (QD) size effect on device properties was studied. With the introduction of CdSe/ZnS and InP/ZnS quantum dots into solar cells, efficiency values higher than 30% are expected for dot sizes higher than 2.2 nm, which is a result of an increased current density due to a higher absorption of photons in quantum dots while voltage output is almost independent on dot size. In particular, maximum efficiency values of 31.73% and 32.90% are obtained for CdSe/ZnS and InP/ZnS, respectively under full concentrated light for a dot size of 2.3 nm, thereby demonstrating the potentiality of these proposed heterostructures. However, it is important to point out that quantum dot size is a critical parameter to be controlled since with dot size reduction to 1.1 nm the efficiency is decreased to 7%. As a result, this work reveals that quantum dots size constitutes an important parameter to be controlled that impacts on the generated current density.

Acknowledgments

DL and MP thanks partial financial support from FONDECYT 1 180 905. DL thanks partial financial support from Centers of excellence with BASAL/ANID financing, AFB180001, CEDENNA.

ORCID iDs

Asmae El Aouami https://orcid.org/0000-0001-6830-8106
Francis Dujardin https://orcid.org/0000-0001-8754-1106
David Laroze https://orcid.org/0000-0002-6487-8096
Mimoun Zazoui https://orcid.org/0000-0003-2739-628X
El Mustapha Feddi https://orcid.org/0000-0001-6641-3623

References

[1] Shockley W and Queisser H J 1961 Detailed balance limit of efficiency of p-n junction solar cells *J. Appl. Phys.* **32** 510–9
[2] Landsberg P and Tonge G 1980 Thermodynamic energy conversion efficiencies *J. Appl. Phys.* **51** R1–20
[3] Green M A 2006 *Third Generation Photovoltaics* (Berlin: Springer)
[4] Green M A 2001 Third generation photovoltaics: ultra-high conversion efficiency at low cost *Prog. Photovoltaics Res. Appl.* **9** 123–35
[5] Luque A and Martí A 1997 Increasing the efficiency of ideal solar cells by photon induced transitions at intermediate levels *Phys. Rev. Lett.* **78** 5014
[6] Martí A, Antolín E, Stanley C, Farmer C, López N, Díaz P, Cánovas E, Linares P and Luque A 2006 Production of photocurrent due to intermediate-to-conduction-band transitions: A demonstration of a key operating principle of the intermediate-band solar cell *Phys. Rev. Lett.* **97** 247701

[7] Shao Q, Balandin A, Fedoseyev A and Turowski M 2007 Intermediate-band solar cells based on quantum dot supracrystals *Appl. Phys. Lett.* **91** 163503
[8] Oshima R, Takata A and Okada Y 2008 Strain-compensated inas/ganas quantum dots for use in high-efficiency solar cells *Appl. Phys. Lett.* **93** 083111
[9] Martí A, Lopez N, Antolin E, Canovas E, Luque A, Stanley C, Farmer C and Diaz P 2007 Emitter degradation in quantum dot intermediate band solar cells *Appl. Phys. Lett.* **90** 233510
[10] Soga T 2006 *Nanostructured Materials for Solar Energy Conversion* (Amsterdam: Elsevier)
[11] Wu J and Wang Z M 2014 *Quantum Dot Solar Cells* (Berlin: Springer)
[12] Ramiro I and Martí A 2020 Intermediate band solar cells: Present and future *Prog. Photovoltaics Res. Appl.* 1–9
[13] Zhang Q and Wei W 2013 Single intermediate-band solar cells of ingan/inn quantum dot supracrystals *Appl. Phys.* A **113** 75–82
[14] Vurgaftman I, Meyer J Á and Ram-Mohan L Á 2001 Band parameters for iii-v compound semiconductors and their alloys *J. Appl. Phys.* **89** 5815–75
[15] Jenks S and Gilmore R 2010 Quantum dot solar cell: materials that produce two intermediate bands *J. Renewable Sustainable Energy* **2** 013111
[16] El Aouami A, Feddi K, El Haouari M, El Yadri M, Afkir N B, Zazoui M, Feddi E, Duque C and Dujardin F 2019 Impact of heavy hole levels on the photovoltaic conversion efficiency of $In_xGa_{1-x}N$/InN quantum dot intermediate band solar cells *Superlattices Microstruct.* **129** 202–11
[17] El Aouami A, Bikerouin M, El-Yadri M, Feddi E, Dujardin F, Courel M, Chouchen B, Gazzah M and Belmabrouk H 2020 Internal polarization electric field effects on the efficiency of InN/$In_xGa_{1-x}N$ multiple quantum dot solar cells *Sol. Energy* **201** 339–47
[18] Aly A E-M M and Nasr A 2014 Theoretical performance of solar cell based on mini-bands quantum dots *J. Appl. Phys.* **115** 114311
[19] Aly A E-M M and Nasr A 2015 The effect of multi-intermediate bands on the behavior of an inas1- xnx/gaas1- ysby quantum dot solar cell *J. Semicond.* **36** 042001
[20] Chowdhury I U I, Sarker J, Shifat A Z, Shuvro R A and Mitul A F 2018 Performance analysis of high efficiency inxga1- xn/gan intermediate band quantum dot solar cells *Results in Physics* **9** 432–9
[21] Deng Q, Wang X, Yang C, Xiao H, Wang C, Yin H, Hou Q, Li J, Wang Z and Hou X 2011 Theoretical study on inxga1- xn/gan quantum dots solar cell *Physica B* **406** 73–6
[22] Luque A, Martí A, López N, Antolin E, Cánovas E, Stanley C, Farmer C, Caballero L, Cuadra L and Balenzategui J 2005 Experimental analysis of the quasi-fermi level split in quantum dot intermediate-band solar cells *Appl. Phys. Lett.* **87** 083505
[23] Antolin E, Martí A, Linares P G, Ramiro I, Hernández E, Farmer C, Stanley C and Luque A 2010 Advances in quantum dot intermediate band solar cells *2010 XXXV IEEE Photovoltaic Specialists Conf. (IEEE)* pp 000065–70
[24] Lantratov V M, Mintairov S A, Blokhin S A, Kalyuzhnyy N A, Ledentsov N N, Maximov M V, Nadtochiy A M, Pauysov A S, Sakharov A V and Shvarts M Z 2010 Algaas/gaas photovoltaic cells with ingaas quantum dots *Advances in Science and Technology* vol 74 (Switzerland: Trans Tech Publ) pp 231–6
[25] Popescu V, Bester G, Hanna M C, Norman A G and Zunger A 2008 Theoretical and experimental examination of the intermediate-band concept for strain-balanced (in, ga) as/ga (as, p) quantum dot solar cells *Phys. Rev.* B **78** 205321
[26] Hubbard S M, Bailey C G, Cress C D, Polly S, Clark J, Forbes D V, Raffaelle R P, Bailey S G and Wilt D M 2008 Short circuit current enhancement of gaas solar cells using strain compensated inas quantum dots *2008 XXXIII IEEE Photovoltaic Specialists Conf. (IEEE)* pp 1–6
[27] Ramiro I, Villa J, Tablero C, Antolín E, Luque A, Martí A, Hwang J, Phillips J, Martin A and Millunchick J 2008 Analysis of the intermediate-band absorption properties of type-ii gasb/gaas quantum-dot photovoltaics *Phys. Rev.* B **96** 125422
[28] Shen Q, Kobayashi J, Diguna L J and Toyoda T 2008 Effect of zns coating on the photovoltaic properties of cdse quantum dot-sensitized solar cells *J. Appl. Phys.* **103** 084304
[29] Shen G, Harris N, Dawahre N, Wilbert D S, Baughman W, Rivera E, Nikles D, Bryant T L, Kim S M and Kung P 2011 Inp/zns core-shell quantum dots sensitized zno nanowires for photovoltaic devices *2011 International Semiconductor Device Research Symposium (ISDRS) (IEEE)* pp 1–2
[30] Zavaraki A J, Liu Q and Ågren H 2020 Solar cell sensitized with 'green' inp-zns quantum dots: Effect of zns shell deposition *Nano-Structures & Nano-Objects* **22** 100461
[31] Lazarenkova O L and Balandin A A 2001 Miniband formation in a quantum dot crystal *J. Appl. Phys.* **89** 5509–15
[32] BenDaniel D and Duke C 1966 Space-charge effects on electron tunneling *Phys. Rev.* **152** 683
[33] El Aouami A, Feddi E, Talbi A, Dujardin F and Duque C 2018 Electronic state and photoionization cross section of a single dopant in GaN/InGaN core/shell quantum dot under magnetic field and hydrostatic pressure *Appl. Phys.* A **124** 442
[34] Van Roosbroeck W and Shockley W 1954 Photon-radiative recombination of electrons and holes in germanium *Phys. Rev.* **94** 1558
[35] Bastard G 1982 Theoretical investigations of superlattice band structure in the envelope-function approximation *Phys. Rev.* B **25** 7584
[36] Adachi S 2009 (*Properties of Semiconductor Alloys: Group-IV, III-V and II-VI Semiconductors* vol 28) (New York: Wiley)
[37] Levy M Y, Honsberg C, Martí A and Luque A 2005 Quantum dot intermediate band solar cell material systems with negligible valence band offsets *Conf. Record of the Thirty-first IEEE Photovoltaic Specialists Conf.* (2005) *(IEEE) pp 90–3*